nature nanotechnology

LETTERS

PUBLISHED ONLINE: 3 JULY 2011 | DOI: 10.1038/NNANO.2011.96

Interfacial phase-change memory

R. E. Simpson[1]*, P. Fons[1,2], A. V. Kolobov[1,2], T. Fukaya[1], M. Krbal[1], T. Yagi[3] and J. Tominaga[1]*

Phase-change memory technology relies on the electrical and optical properties of certain materials changing substantially when the atomic structure of the material is altered by heating[1] or some other excitation process[2–5]. For example, switching the composite $Ge_2Sb_2Te_5$ (GST) alloy from its covalently bonded amorphous phase to its resonantly bonded metastable cubic crystalline phase decreases the resistivity by three orders of magnitude[6], and also increases reflectivity across the visible spectrum[7,8]. Moreover, phase-change memory based on GST is scalable[9–11], and is therefore a candidate to replace Flash memory for non-volatile data storage applications. The energy needed to switch between the two phases depends on the intrinsic properties of the phase-change material and the device architecture; this energy is usually supplied by laser or electrical pulses[1,6]. The switching energy for GST can be reduced by limiting the movement of the atoms to a single dimension, thus substantially reducing the entropic losses associated with the phase-change process[12,13]. In particular, aligning the *c*-axis of a hexagonal Sb_2Te_3 layer and the ⟨111⟩ direction of a cubic GeTe layer in a superlattice structure creates a material in which Ge atoms can switch between octahedral sites and lower-coordination sites at the interface of the superlattice layers. Here we demonstrate $GeTe/Sb_2Te_3$ interfacial phase-change memory (IPCM) data storage devices with reduced switching energies, improved write-erase cycle lifetimes and faster switching speeds.

A physical vapour deposition system was used to grow GeTe–Sb_2Te_3 superlattices with GeTe and Sb_2Te_3 layer thicknesses between 5 Å and 40 Å (herein named interfacial phase-change materials, IPCM). Figure 1a presents a typical example of an IPCM structure grown on an oxidized silicon wafer. The local atomic structure transformed into the cubic crystalline phase at a temperature of 155 ± 10 °C, which is consistent with the crystallization temperature of the $Ge_2Sb_2Te_5$ (GST) composite alloy[6,10,14], but lower than the crystallization temperature of GeTe confined within thicker multilayer structures (190–250 °C)[15].

In the somewhat random local atomic structure of amorphous GST, Ge atoms can occupy both threefold and tetrahedral sites[16,17] (see Supplementary Fig. S1) with principally covalent bonding; this bonding phase is technologically known as the RESET state. In contrast, the cubic crystalline phase is assembled from approximately octahedral sub-units, which are usually described as being 'resonantly' bonded[7,8,18]; this bonding phase is technologically known as the SET state. Given the absence of significant long-range order in nanoscale structures, it is appropriate to discuss the different phases of the IPCM in terms of the bonding nature rather than as being amorphous or crystalline. Herein, the covalent (RESET) and resonant (SET) bonding states will be used when referring to these two phases.

To determine the maximum rate at which data can be written to phase-change random access memory (PCRAM) devices, it is necessary to determine the switching time between the covalently and resonantly bonded phases. The switching time for GST and IPCM samples was measured optically using a laser pump–probe static tester system (see Methods). Figure 1b shows the change in the intensity of the probe light through laser RESET areas in the IPCM film as a function of time during and after the application of a 100 ns pump pulse. Four different regions are discernible: (i) no change in transmission, (ii) a reduction in transmission (indicative of a RESET to SET transition), (iii) an increase in transmission and then, after 100 ns, subsequent crystallization (indicative of a melt-SET transition) and (iv) a two-step transmission increase, which indicates melting and subsequent partial ablation. The plot shows that, for higher laser pump powers, the IPCM could transform into the SET phase in just 25 ns, but continued heating by the 100 ns pulse caused melting and subsequent ablation. In contrast, complete crystallization into the SET phase of the GST film was only observed when the pulse length was increased to at least 80 ns under otherwise identical conditions. Figure 1c also shows that, for low-power laser pulses (9.5 mW in this case), the transition rate of the IPCM to the SET phase is approximately four times greater than that of the GST film. Higher-power (16.5 mW) and shorter pulses with a duration of 25 ns significantly shortened the period of time before crystal growth commenced and allowed complete crystallization without subsequent damage. It should be mentioned that similar enhancements in switching performance were observed in IPCM digital versatile disc measurements (Supplementary Fig. S2).

The transition rate to the resonant (SET) phase is dependent on the structure of the covalent (RESET) phase, which is influenced by the preparation conditions[19,20]. Density function theory (DFT) modelling has shown that quenching GST from a molten state produces a covalent phase where the Ge atoms occupy a mixture of octahedral and lower coordination sites[21,22]. Crystallization then proceeds from the pre-existing octahedral configurations embedded within the covalent phase[21,23]. This is most evident in the crystallization time of sputter-deposited, covalent GST films, which is significantly longer than that of laser melt-quenched[11,24] GST films. Essentially, as-deposited GST films require additional time to form the octahedral structural sub-units, which seed subsequent crystallization[21,23] into the cubic phase. This implies the existence of an optimum covalent GST structure that incorporates sufficient octahedral seeds for efficient crystallization.

The covalent IPCM nanostructures consist of atomic planes of covalently bonded Ge atoms separated by planes of crystalline $R\bar{3}m$ Sb_2Te_3. Applying simplified models for the idealized phase-transition process[8,12], one can speculate that all Ge atoms are located at the Sb_2Te_3 interface. During the phase transition, this interface allows the Ge atoms to switch into the resonantly bonded octahedral sites and it can, therefore, be considered a plane of octahedral nucleation centres, which provides a template[23]

[1]Nanoelectronics Research Institute, National Institute of Applied Industrial Science and Technology, Tsukuba Central 4, 1-1-1 Higashi, Tsukuba 305-8562, Japan, [2]SPring-8, Japan Synchrotron Radiation Research Institute (JASRI), Mikazuki Hyogo 679-5198, Japan, [3]National Metrology Institute of Japan, National Institute of Advanced Industrial Science and Technology, Tsukuba Central 3, 1-1-1 Umezono, Tsukuba, Ibaraki 305-8563, Japan. *e-mail: robert.simpson@aist.go.jp; j-tominaga@aist.go.jp

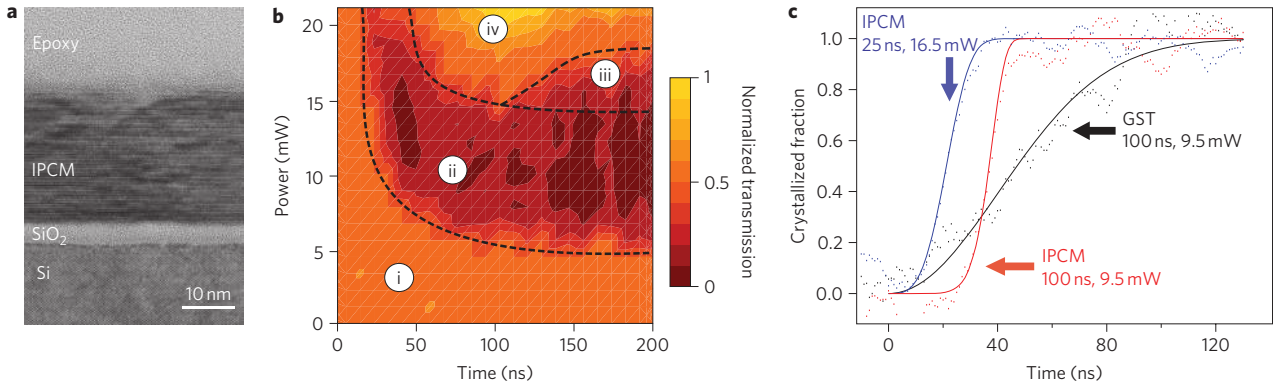

Figure 1 | Optical pump-probe testing of IPCM switching behaviour. a, High-resolution transmission electron micrograph TEM image of a typical as-grown $(GeTe)_2(Sb_2Te_3)_4$ interfacial phase-change material on silicon. The $(GeTe)_2$ layers are 1 nm thick, and the $(Sb_2Te_3)_4$ layers are 4 nm thick. **b**, Time-resolved pump–probe static tester measurement for the RESET to SET transition process of a 400-nm-radius laser RESET mark in the IPCM film. The RESET mark was created with a laser pulse with a duration of 40 ns and a power of 32 mW. The normalized optical transmission of a 100 μW probe beam through the RESET mark is plotted as a function of time during and after the 100 ns laser pump pulse for varying incident optical powers. Four regions can be discerned: (i) no change in transmission, (ii) a reduction in transmission (indicative of a transition from the RESET state to the SET state), (iii) a slight increase followed by a reduction in transmission (indicative of melting then subsequent crystallization into the SET state), and (iv) an increase in transmission (indicative of melting then partial ablation). **c**, Re-crystallized fraction of the 400-nm-radius RESET mark (created with a 40 ns, 32 mW laser pre-pulse) as a function of time for GST (100 ns, 9.5 mW pump pulses; black); IPCM (100 ns, 9.5 mW pump pulses; red); IPCM (25 ns, 16.5 mW pump pulses; blue), respectively.

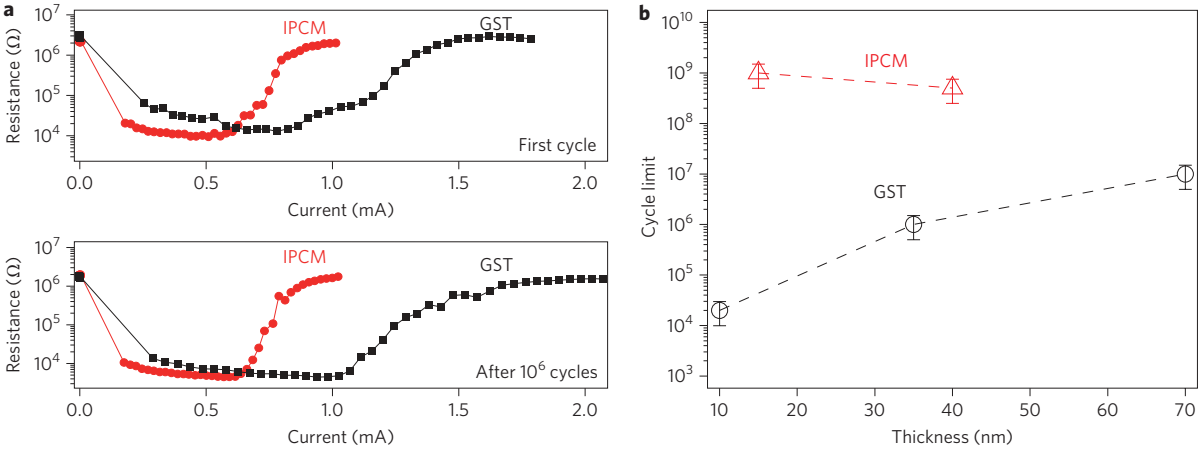

Figure 2 | Electrical switching characteristics of IPCM devices. a, Plots of resistance versus current for PCRAM devices in the first cycle (upper panel) and after 1×10^6 cycles (lower panel). Filled squares are from a device fabricated from a single GST target, and filled circles are for a device containing a $(GeTe)_4(Sb_2Te_3)_2$ IPCM. The SET pulse lengths were 50 ns and 100 ns for the IPCM and GST materials, respectively. The RESET pulse length was fixed at 50 ns for both the IPCM- and GST- based devices. **b**, Maximum number of SET–RESET cycles plotted as a function of phase-change material thickness. The cyclability of phase-change memory cells based on the GST material shows a strong dependence on film thickness (black circles), whereas the cyclability of the IPCM (red triangles) based on repeated blocks of $(GeTe)_2(Sb_2Te_3)_2$ shows little sensitivity to total film thickness. Dashed lines have been included to guide the eye.

for enhanced cubic crystal growth. It should be noted that the covalent and resonantly bonded IPCM structures are stable when relaxed according to DFT calculations.

The homogeneous nature of the IPCM means that each Ge atom experiences the same force, so, for the ideal interface, the distribution of transition energies required by the Ge atoms is a delta function. This allows a fast, coherent switching motion into the octahedral sites when the threshold energy is acquired from either laser irradiation or Joule heating, hence the abrupt IPCM crystallization process observed in Fig. 1c. In contrast, re-amorphized GST is less ordered, so the Ge atoms experience different forces, resulting in a broad distribution of transition energies. A long crystallization pulse (>80 ns) was therefore necessary to completely switch all of the Ge atoms. The point at which crystal growth begins is dependent on the covalent structure and laser power. For the IPCM covalent structure, the Sb_2Te_3 layers provide pre-existing nucleation interfaces that facilitate crystal growth without the time-consuming crystal nucleation process, so complete crystallization is possible in just 25 ns. It was not possible to crystallize amorphous marks in the GST film with such short pulse lengths.

So far, pump–probe techniques have allowed us to corroborate the superior switching and energy performance of GeTe–Sb_2Te_3 nanostructured IPCMs. However, to see the true potential of this enhanced material it is necessary to demonstrate its utilization in real data storage devices. Here, the discussion turns to electrical solid-state memory cells where low-energy, high-speed operation is essential for environmentally friendly data storage.

In Fig. 2a the resistance R of IPCM- and GST-based PCRAM cells is plotted against the applied electric current I. The plot clearly shows that the currents necessary to reversibly switch IPCM-based devices between the SET and RESET states are

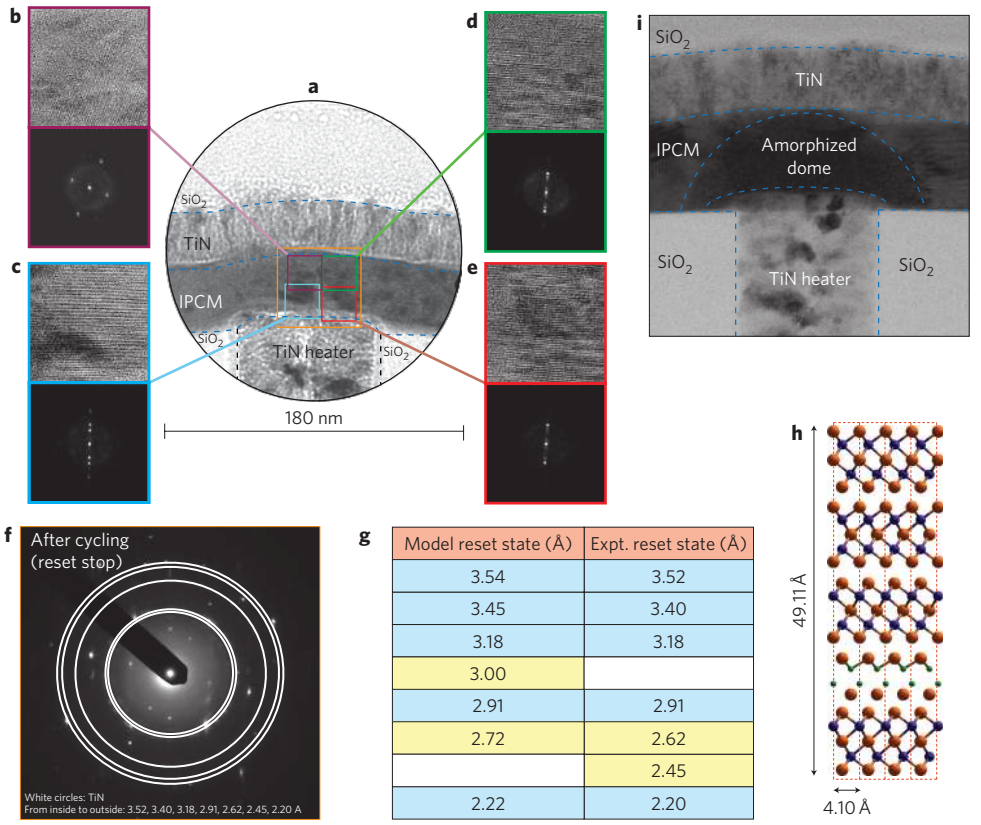

Model reset state (Å)	Expt. reset state (Å)
3.54	3.52
3.45	3.40
3.18	3.18
3.00	
2.91	2.91
2.72	2.62
	2.45
2.22	2.20

Figure 3 | Analysis of the RESET state. a, TEM images of a $(GeTe)_2(Sb_2Te_3)_4$ IPCM structure in the RESET state after 1×10^3 SET–RESET cycles. In contrast to GST, the TEM image shows that there is no amorphous region surrounding the TiN heating electrode. **b**–**e**, High-resolution TEM images (top) and SAD patterns (bottom) for the four regions inside the coloured squares in **a**. The layered IPCM structure and associated superlattice diffraction spots are clearly visible in all images. **f**, Selective area electron diffraction pattern of the whole IPCM structure. The white concentric rings originate from the TiN electrodes. **g**, DFT calculations of the inter-planar distances in $(GeTe)_2(Sb_2Te_3)_4$ (left column) are in good agreement with the distances determined from the diffraction pattern. **h**, Model used in DFT calculations: Ge, Sb and Te atoms are coloured green, purple and orange, respectively. **i**, An IPCM device that was deliberately RESET with the same high-power pulse conditions required by GST. As with GST, a melt-amorphized dome is formed above the TiN heater, resulting in destruction of the superlattice structure and irreversible damage to the IPCM device.

substantially lower than those required for identical devices based on GST. Indeed, the electrical energy used to SET the GST and IPCM devices was 90 pJ and 11 pJ, respectively. Furthermore, due to the homogeneity of the Ge switching environment, the switch (or 'current snap') between the SET and RESET states was substantially more abrupt for the IPCM cells. This produced a tighter distribution of device characteristics, thus facilitating accurate determination of the SET and RESET states.

It is tempting to explain these improvements in device characteristics as a result of increased thermal confinement due to the layered nature of the IPCM structure[25]. The thermal conductivity of both IPCM and GST films was directly measured by a standard pump–probe, thermoreflectivity technique[26], the most suitable technique available for measuring thermal conductivity perpendicular to the surface of thin-film materials. In contrast with thicker multilayered phase-change films[27], heat was found to diffuse through the IPCM faster than that for an otherwise identical film deposited from a composite target (Supplementary Fig. S3). This implies that the thermal boundary resistance between the individual Sb_2Te_3 and GeTe layers is negligible[25]. The actual thermal conductivities were calculated to be $0.33\ Wm^{-1}K^{-1}$ for the IPCM and $0.21\ Wm^{-1}K^{-1}$ for the GST film. These measurements explicitly show that the enhanced phase-change performance of IPCM cannot be explained by reduced thermal conductivity.

Entropy arguments, however, can explain the efficiency improvements observed for IPCM. The crystallization process in GST is three-dimensional; that is, atomic movements occur stochastically in all directions[21]. The covalent state is composed of a range of local atomic configurations[16], so it has a relatively large entropy. In contrast, the IPCM structures, reported here, were designed to minimize the change in configurational entropy between SET and RESET states. The ultrathin, uniform stratum of Sb_2Te_3 and GeTe lowers the entropy of the covalent state by restricting the number of atomic configurations that can exist. For the SET operation, IPCM-based devices use just 12% of the energy required by similar GST-based devices, an improvement consistent with the theoretical efficiency enhancement[13]. This increase in efficiency means that less energy is wasted during the phase transition, which in turn leads to more than an order of magnitude improvement in the SET–RESET cyclability[11]. The enhanced cyclability is most clear in Fig. 2b, which shows the number of times the GST and IPCM PCRAM cells could be cycled before failure for films of different thicknesses. The IPCM cycling performance shows little dependence on film thickness, but the cycling performance of the GST cell diminishes as the film thickness is reduced. These significant increases in device performance were only possible for Sb_2Te_3–GeTe interfaces with crystallographic texture normal to the substrate; poor-quality interfaces with multiple grains required substantially higher SET ↔ RESET switching energies and resulted in fewer cycles being completed before failure.

Reducing the entropic losses has the further ramification of producing device characteristics that are highly repeatable. Indeed, the

resistance of the IPCM during the first SET–RESET cycle is identical to that of the millionth cycle (see Fig. 2a). This implies that the IPCM structure is sustained for at least one million write–erase cycles. In contrast, as-deposited GST cells require more than 100 cycles before the structures of the SET and RESET states settle to give reproducible resistances; this is typical for GST[28,29]. The structure of the IPCM device in the RESET state after extended cycling is shown in Fig. 3a. The amorphous dome-shaped region is absent and, more importantly, a closer inspection of the IPCM directly above the heating electrode (Fig. 3b–e), reveals that the structure remains ordered in layers. Selective area diffraction (SAD) patterns associated with these images similarly display superlattice reflections, thus proving that, even after cycling, the layer structure is still present. In Fig. 3b, the direction of the layers is at a slight angle with respect to the growth plane. This tends to occur for thicker films above the corner of the heater plug and can be avoided for thinner IPCM films. The SAD pattern collected from the whole IPCM structure (Fig. 3f) confirms the overall crystallinity of the cell. Interplanar distances calculated from the diffraction spots show excellent agreement with DFT models of Ge atoms in a low-coordination state at the Sb_2Te_3–GeTe interface (Fig. 3g,h), indicating a non-melting transition of the Ge atoms. In contrast, the RESET state of GST-based PCRAM cells exhibits a dome-shaped amorphous region above the heating electrode that results from melt-quenching during the RESET process[11]. For the purpose of comparison, Fig. 3i shows an IPCM cell that was deliberately RESET with the same high-power electrical pulse conditions required by GST (1.25 mA at 6 V for 50 ns). As with GST, a dome-shaped melt-amorphized region formed above the TiN heating electrode. Resetting with such large electrical currents destroyed the IPCM superlattice structure and the device therefore required much larger SET and RESET currents for further switching operations.

For GST it is generally accepted that atomic diffusion towards the memory cell's electrodes is a major cause of device failure[30,31]. Because the atoms within a thin phase-change film need only diffuse over a relatively short distance in order to meet the cell's electrodes, one would expect thinner phase-change films to fail with fewer cycles than thicker films; this dependency is demonstrated for the GST samples shown in Fig. 2b. The IPCM cells, however, do not show any strong dependence on film thickness, and even films 15 nm thick can be switched between the SET and RESET states more than one billion times, a characteristic that will become increasingly important as memory cells are further reduced in size to meet the demands of higher data storage densities. In contrast, GST devices of a similar thickness fail within 20,000 SET–RESET cycles. These measurements, in combination with the negligible changes in electrical resistance during cycling, the lack of an amorphous dome at the heating electrode and the cycle durability of the layered structure provide substantial evidence that interlayer diffusion is negligible in the IPCM structure. These results are consistent with recent *in situ* measurements of excitation-assisted amorphization in GST[3] and other chalcogenides[32–34], switching models based on resonant bonding arguments[5,8,18] and ultrafast, low-energy optical manipulation of atomic arrangements in IPCM structures[4], all of which occur without melting in the conventional sense. In contrast to GST memory cells, which due to repeated switching-induced melting tend to show migration of Ge and Sb atoms towards the cathode and Te towards the anode[30], composition analysis of the cycled IPCM cell did not show migration of the atomic species (see the energy-dispersive X-ray spectroscopy data in the Supplementary Information). This observation is consistent with a non-melting IPCM RESET operation as well as reported measurements of substantially reduced atomic diffusivities in the electrically stressed solid films of GST[31].

Despite the apparent similarities between the IPCM and other layered (superlattice-like) phase-change structures[15,27], the difference in the materials' operation is clear when one compares the performance within a device. The IPCM devices used for the electrical switching measurements shown in Fig. 2a consisted of GeTe layers less than 2 nm thick, so all Ge atoms were close to an Sb_2Te_3 interface. Consequently, a single SET event is observed for the IPCM, and the Sb_2Te_3 layers act as inert crystalline seeding layers. In contrast, the thicker layers within the superlattice-like structures show independent crystallization events for the GeTe and Sb_2Te_3 layers[15]. The IPCM-based devices also show two orders of magnitude change in resistance (same as for GST-based devices), whereas the superlattice-like structures show one order of magnitude change[15]. Furthermore, the change in configurational entropy has been minimized for the IPCM, so its SET current is an order of magnitude lower than that reported for the superlattice-like structures[15,27], a result that is in good agreement with calculated efficiency enhancements[13].

The SET process for the PCRAM devices and static tester measurements show that significant efficiency enhancements are possible by implementing an IPCM structure. In particular, compared with GST, the IPCM nanostructure uses an order of magnitude less energy for the SET operation. These results, in conjunction with the fact that the IPCM structure can withstand repeated cycling, indicate that the enhanced IPCM device performance is correlated with a reduced entropy difference between the SET and RESET states. Switching between these states is possible without melting the IPCM structure, so the probability of long-range atomic diffusion and associated damage to the device is reduced. The lower energy consumption of the IPCM switching process results in a correlated[11] order of magnitude increase in the SET–RESET cycle endurance ($>1 \times 10^7$ cycles) when compared with GST ($<2 \times 10^6$ cycles). We have also found that thicker Sb_2Te_3 layers do not significantly influence the rate of crystallization but can reduce the stress during the switching process, thus allowing switching at even lower energies and further increases in the number of SET–RESET cycles. Supplementary Table 1 summarizes the main measurements performed on both GST and IPCM materials.

In conclusion, the interface between the GeTe and Sb_2Te_3 controls the local atomic switching of Ge atoms resulting in a phase transition with substantially reduced entropic losses. As a result, the IPCM RAM devices consume an order of magnitude less energy during the SET process and show enhanced switching responsiveness with respect to their GST counterpart. On the basis of these results we believe the most efficient and fastest phase-change memory devices will be developed using nano-structured materials that take advantage of entropy controlled switching and, furthermore, exhibit effective electrical properties that are unattainable in GST. This work has introduced further degrees of freedom to tailor the performance of the data storage devices on which the modern world has become reliant.

Methods

For the static tester measurement, a dual laser system was used to measure the switching time of the IPCM and GST materials. The transmitted intensity of the probe laser beam (633 nm) was measured while the same spot on the film was excited by a pulsed 650 nm pump laser. Owing to the substantial differences in the transmittance of the films between the resonant and covalent bonding states, the transmitted intensity of the probe was assumed to decrease in proportion to the fraction of the resonantly bonded phase, and a relative comparison of the transition rate is possible by fitting the data using a Johnson–Mehl–Avrami–Kolmogorov-like equation[35], which describes the kinetics of solid-state phase transformations. For the 100 ns, 9.5 mW pump pulse, the rate of crystal growth from the RESET state for the IPCM was more than four times greater than for the GST film irradiated with an identical pulse (Fig. 1c). Further details are given in the Supplementary Information.

PCRAM cells based on a 75 nm TiN heating electrode (Fig. 3a) containing both standard GST and IPCM films were compared in terms of device performance. Figure 2a shows that the cells were initially in the high-resistance covalent state. PCRAM cells using GST switched from the covalent (RESET) to resonant (SET) bonding states by driving a current of 0.3 mA with a 3 V pulse for 100 ns (90 pJ). In stark contrast, the same operation was possible in identical PCRAM cells containing

the IPCM material by supplying a current of 0.15 mA with a 1.5 V pulse for 50 ns (11 pJ). It should be noted that it was possible to SET IPCM devices with shorter pulse durations and therefore the IPCM devices switching energy consumption should be considered a conservative estimate. Similarly, improvements in device efficiency were also possible for the RESET operation, with 0.73 mA at 3.5 V for 50 ns being required for the IPCM cells, compared with 1.25 mA at 6 V for 50 ns for GST-based cells. Further measurement details are given in the Supplementary Information.

Received 25 March 2011; accepted 23 May 2011; published online 3 July 2011

References

1. Wuttig, M. & Yamada, N. Phase-change materials for rewriteable data storage. *Nature Mater.* **6,** 824–832 (2007).
2. Karpov, I. V., Mitra, M., Kau, D., Spadini, G., Kryukov, Y. A., & Karpov, V. G. Evidence of field induced nucleation in phase change memory. *Appl. Phys. Lett.* **92,** 173501 (2008).
3. Fons, P. *et al.* Photoassisted amorphization of the phase-change memory alloy $Ge_2Sb_2Te_5$. *Phys. Rev. B* **82,** 041203 (2010).
4. Makino, K., Tominaga, J. & Hase, M. Ultrafast optical manipulation of atomic arrangements in chalcogenide alloy memory materials. *Opt. Express* **19,** 1260–1270 (2011).
5. Kolobov, A. V., Krbal, M., Fons, P., Tominaga, J., & Uruga, T. Distortion-triggered loss of long-range order in solids with bonding energy hierarchy. *Nature Chem.* **3,** 311–316 (2011).
6. Lankhorst, M., Ketelaars, B. & Wolters, R. Low-cost and nanoscale non-volatile memory concept for future silicon chips. *Nature Mater.* **4,** 347–352 (2005).
7. Shportko, K., Kremers, S., Woda, M., Lencer, D., Robertson, J. & Wuttig, M. Resonant bonding in crystalline phase-change materials. *Nature Mater.* **7,** 653–658 (2008).
8. Huang, B. & Robertson, J. Bonding origin of optical contrast in phase-change memory materials. *Phys. Rev. B* **81,** 081204R (2010).
9. Pirovano, A., Lacaita, A. L., Benvenuti, A., Pellizzer, F., Hudgens, S. & Bez, R. Scaling analysis of phase-change memory technology. *IEDM Technical Digest* 29.6.1–29.6.4 (2003).
10. Simpson, R. E. *et al.* Toward the ultimate limit of phase change in $Ge_2Sb_2Te_5$. *Nano. Lett.* **10,** 414–419 (2010).
11. Burr, G. W. *et al.* Phase change memory technology. *J. Vac. Sci. Technol. B* **28,** 223–262 (2010).
12. Kolobov, A., Fons, P., Frenkel, A., Ankudinov, A., Tominaga, J., and Uruga, T. Understanding the phase-change mechanism of rewritable optical media. *Nature Mater.* **3,** 703–708 (2004).
13. Tominaga, J., Simpson, R., Fons, P. & Kolobov, A. Phase change meta-material and device characteristics. *Proc. Europ. Symp. Phase Change and Ovonic Science*, 54–59 (2010).
14. Yamada, N., Ohno, E., Nishiuchi, K., Akahira, N. & Takao, M. Rapid phase-transitions of GeTe–Sb_2Te_3 pseudobinary amorphous thin-films for an optical disk memory. *J. Appl. Phys.* **69,** 2849–2856 (1991).
15. Chong, T. C. *et al.* Crystalline amorphous semiconductor superlattice. *Phys. Rev. Lett.* **100,** 136101 (2008).
16. Krbal, M. *et al.* Intrinsic complexity of the melt-quenched amorphous $Ge_2Sb_2Te_5$ memory alloy. *Phys. Rev. B* **83,** 054203 (2011).
17. Akola, J. *et al.* Experimentally constrained density-functional calculations of the amorphous structure of the prototypical phase-change material $Ge_2Sb_2Te_5$. *Phys. Rev. B* **80,** 020201 (2009).
18. Simpson, R., Fons, P., Wang, X., Kolobov, A. V., Fukaya, T. & Tominaga, J. Nonmelting super-resolution near-field apertures in Sb–Te alloys. *Appl. Phys. Lett.* **97,** 161906 (2010).
19. Kwon, M-H. *et al.* Nanometer-scale order in amorphous $Ge_2Sb_2Te_5$ analyzed by fluctuation electron microscopy. *Appl. Phys. Lett.* **90,** 021923 (2007).
20. Lee, B-S. *et al.* Observation of the role of subcritical nuclei in crystallization of a glassy solid. *Science* **326,** 980–984 (2009).
21. Hegedüs, J. & Elliott, S. Microscopic origin of the fast crystallization ability of Ge–Sb–Te phase-change memory materials. *Nature Mater.* **7,** 399–405 (2008).
22. Akola, J. & Jones, R. Binary alloys of Ge and Te: order, voids, and the eutectic composition. *Phys. Rev. Lett.* **100,** 205502 (2008).
23. Hegedus, J. & Elliott, S. R. Computer-simulation design of new phase-change memory materials. *Phys. Status Solidi A* **207,** 510–515 (2010).
24. Weidenhof, V., Friedrich, I., Ziegler, S. & Wuttig, M. Laser induced crystallization of amorphous GeSbTe films. *J. Appl. Phys.* **89,** 3168–3176 (2001).
25. Chen, G. Thermal conductivity and ballistic-phonon transport in the cross-plane direction of superlattices. *Phys. Rev. B* **57,** 14958–14973 (1998).
26. Taketoshi, N., Baba, T. & Ono, A. Development of a thermal diffusivity measurement system for metal thin films using a picosecond thermoreflectance technique. *Meas. Sci. Technol.* **12,** 2064–2073 (2001).
27. Chong, T. *et al.* Phase change random access memory cell with superlattice-like structure. *Appl. Phys. Lett.* **88,** 122114 (2006).
28. Lai, S. & Lowrey, T. OUM – a 180 nm nonvolatile memory cell element technology for stand alone and embedded application. *IEDM Technical Digest* 36.5.1–36.5.4 (2001).
29. Chen, K-N. & Krusin-Elbaum, L. The fabrication of a programmable via using phase-change material in CMOS-compatible technology. *Nanotechnology* **21,** 134001 (2010).
30. Kim, C. *et al.* Direct evidence of phase separation in $Ge_2Sb_2Te_5$ in phase change memory devices. *Appl. Phys. Lett.* **94,** 193504 (2009).
31. Yang, T-Y., Park, I-M., Kim, B-J. & Joo, Y-C. Atomic migration in molten and crystalline $Ge_2Sb_2Te_5$ under high electric field. *Appl. Phys. Lett.* **95,** 032104 (2009).
32. Poborchii, V. V., Kolobov, A. V., & Tanaka, K. Photomelting of selenium at low temperature. *Appl. Phys. Lett.* **74,** 215–217 (1999).
33. Frumar, M., Firth, A. & Owen, A. Optically induced crystal-to-amorphous-state transition in As_2S_3. *J. Non-Cryst. Solids* **192,** 447–450 (1995).
34. Elliott, S. & Kolobov, A. Athermal light-induced vitrification of $As_{50}Se_{50}$ films. *J. Non-Cryst. Solids* **128,** 216–220 (1991).
35. Málek, J. The applicability of Johnson–Mehl–Avrami model in the thermal analysis of the crystallization kinetics of glasses. *Thermochim. Acta.* **267,** 61–73 (1995).

Acknowledgements

This work was supported by the New Energy and Industrial Technology Development Organization project 'Research and development of nanoelectronic device technology'. The authors thank Elpida Memory Inc. for device measurement discussions, R. Kondo for technical assistance and S. Cook for reading the manuscript. R.E.S. and M.K. would like to thank the Japanese Society for the Promotion of Science for their research fellowships. All work presented here was performed under the auspices of the Center for Applied Near-Field Optics Research (CAN-FOR).

Author contributions

J.T. conceived and designed the entropy controlled interfacial phase-change memory structures. J.T., R.E.S. and T.Y. performed the experiments. R.E.S. wrote the paper. All authors analysed the results and contributed to the discussion presented in the manuscript.

Additional information

The authors declare no competing financial interests. Supplementary information accompanies this paper at www.nature.com/naturenanotechnology. Reprints and permission information is available online at http://www.nature.com/reprints/. Correspondence and requests for materials should be addressed to R.E.S. and J.T.

nature nanotechnology

SUPPLEMENTARY INFORMATION

DOI: 10.1038/NNANO.2011.96

Interfacial phase-change memory

R. E. Simpson,[1,*] P. Fons,[1,2] A. V. Kolobov,[1,2] T. Fukaya,[1] M. Krbal,[1] T. Yagi,[3] and J Tominaga[1,†]

[1] *Nanoelectronics Research Institute, National Institute of Applied Industrial Science and Technology, Tsukuba Central 4, 1-1-1 Higashi, Tsukuba 305-8562, Japan*

[2] *SPring-8, Japan Synchrotron Radiation Research Institute (JASRI), Mikazuki Hyogo 679-5198, Japan*

[3] *National Metrology Institute of Japan, National Institute of Advanced Industrial Science and Technology, Tsukuba Central 3, 1-1-1 Umezono, Tsukuba, Ibaraki 305-8563, Japan*

Growth Procedure.

The IPCM structures were designed to reduce entropic losses by creating the ideal local atomic environment for a one diemnsional transition of Ge atoms (see Fig. S1) at the interface between the Sb_2Te_3 and GeTe superlattice layers. The layer thicknesses were chosen by considering the lattice parameters from published diffraction measurements of GeTe [1] and Sb_2Te_3 [2, 3] and then calculating the minimum thickness in the 1 1 1 direction required to achieve the GeTe and Sb_2Te_3 compositions. The $(GeTe)_2(Sb_2Te_3)$ and $(GeTe)_2(Sb_2Te_3)_4$ IPCMs were fabricated by alternately layering films of these fundamental units.

All films were deposited by helicon-wave RF magnetron sputtering (ULVAC). The distance between the sample holder and the sputtering targets was 200 mm. The sputtering system was equipped with independent targets of Sb_2Te_3, GeTe, and TiN. The target diameters were 50.8 mm. The chamber was evacuated to a pressure of $< 1x10^{-5}$ Pa, and sputtering was carried out at 0.5 Pa, in a high purity Ar ambient. Individual source shutters were alternatively opened and closed for durations determined by the calibrated deposition rate (Å/sec) of each target. The sample holder was held at 250°C for film deposition. X-ray fluorescence measurements revealed less than a 3 at. % deviation from the targeted IPCM average composition. For TiN deposition a gas composition of approximately 5% high purity N_2 in an Ar balance was used. The use of a remote plasma allowed control of layer thickness and prevented plasma damage to the sample surface. Individual source shutters were computer controlled to grow the desired structures. Phase change films were grown on silicon wafers and fused silica substrates for material analysis.

*Electronic address: robert.simpson@aist.go.jp

†Electronic address: j-tominaga@aist.go.jp

PCRAM devices were fabricated by growing phase change materials atop of patterned Si substrates incorporating 70 nm diameter TiN heating electrodes embedded in a SiO_2 matrix. The upper TiN electrodes were deposited *in situ* thus completing the device structure. All PCRAM devices had a phase change material thickness of 40 nm. For the DVD measurements, the samples were grown on polycarbonate substrates at room temperature. A 140 nm $(ZnS)_{0.85}(SiO_2)_{0.15}$ /30 nm Phase Change / 20 nm $(ZnS)_{0.85}(SiO_2)_{0.15}$ /50 nm AlCr stack was used to form the sample structure.

It should be noted that growing $Ge_2Sb_2Te_5$ (GST) with texture along crystallographic axes other than (111) is fraught with difficulties and even using GaSb single crystal substrates with (001) orientation, GST relaxes into a structure with facets along (111) [4]. Similar attempts to grow GST and IPCM with (001) texture using a helicon-wave sputtering system on device substrates also proved unsuccessful.

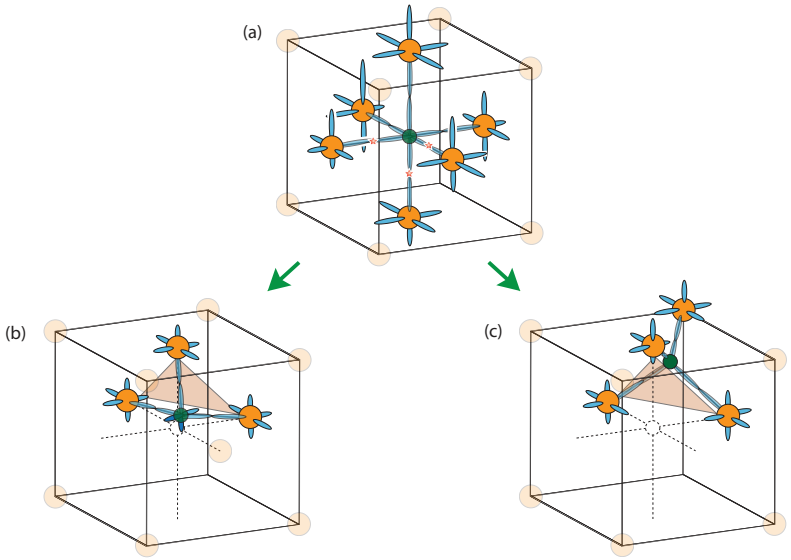

FIG. S1: A key feature of the IPCM is the one dimensional nature of the Ge atom's transition from (a) octahedrally co-ordinated sites with aligned p-orbitals, which result in resonant bonding, to covalently bonded sites of lower coordination. Two possible models are shown that potentially allow for the one-dimensional motion of Ge atoms and account for the observed property enhancement: one is based on the simple breaking of resonant bonds generating Ge(3)Te(3) local structure [13–15] (b) and the other one involves the umbrella-flip generating Ge(4)Te(2) local structure[16, 17]. In both cases the Ge atom is displaced along the $< 111 >$ direction. Te atoms that form bonds to the switching Ge atom are shown in bright orange while those forming the fcc unit cell, but not bonded to the Ge atom in question, are shown in pale orange. Other (Ge and Sb) atoms are not shown for simplicity.

Pump-probe (Static Tester) measurement

A laser static tester system [5, 6] was used to measure the SET and RESET times of the GST and IPCM films. Pump pulses with a maximum optical power (measured at the sample's surface) of 45 mW and duration from 5 ns to 1 μs were used to change the materials phase. The transmission of the probe through the samples was measured using a Hamamatsu avalanche photodiode with a 100 ps resolution. The resolution of the detection system was limited to 1 ns by the 1 GHz bandwidth of the National Instruments data acquisition card. The pump wavelength was 650 nm whilst the probe wavelength was 635 nm. To ensure continuous perfect optical alignment both lasers beams were transmitted through a single mode optical fibre thus allowing the centre of the pumped spot to be probed. A 0.65 NA, $\times$ 40, conjugate achromatic objective lens was used to focus the beams to a spot diameter of $\sim$ 800 nm. The power-time-transmission re-crystallisation plots were created by initially forming a RESET mark with a 40 ns, 32 mW pump pulse and then measuring the transmitted intensity of the probe pulse through the RESET mark for a fixed 100 ns (and 25 ns for the second measurement on the IPCM) pump pulse-time and iteratively increasing the power by 1 mW. The location of each measurement was separated by 5 μm. For each optical pump power, this measurement was repeated 10 times and the average measurement was used to create the plot in Fig. 1(b).

For the analysis of the crystallisation mechanism (Fig. 1(c)), the baseline transmission value for the 100 % crystallised state was taken to be the point that the change in transmission saturated. It is not possible to deduce absolute quantities for the Avrami parameters from the Johnson-Mehl-Avrami-Kolmogorov (JMAK) equation [7] equation since the theory assumes: (i) homogeneous nucleation (ii) spherical crystal nuclei and (iii) the material is under equilibrium conditions. All of these assumptions are not valid for the case of laser heating the IPCM. However, for identical laser pulse conditions the films are heated at the same rate thus relative quantitative comparisons can be made. To distinguish this type of relative JMAK analysis from absolute JMAK analysis, it is referred to as JMAK-like.

DVD Characterisation

Digital Versatile Disc (DVD) measurements were used to demonstrate the enhanced crystallisation speed of the IPCM based discs. Samples were fabricated on DVD polycarbonate substrates. A $(ZnS)_{0.85}(SiO_2)_{0.15}$ insulating layer of 140 nm, a 20 nm phase-change layer, a 20 nm $(ZnS)_{0.85}(SiO_2)_{0.15}$ buffer and a 50 nm AlCr reflective layer were sequentially deposited. The GST reference sample, was fabricated in a Shibaura RF sputtering system (4EP-LL) with a 0.5 Pa argon ambient. For the multilayer samples, a helicon wave sputtering system was used to deposit the phase-change layer at room temperature from individual Sb_2Te_3 and GeTe composite targets. This layer was also deposited in a Ar atmosphere at 0.5 Pa. The target thicknesses of the Sb_2Te_3 and GeTe layers were 5 Å. The multilayer structure consisted of a total of 40 layers resulting in a IPCM approximately 20 nm thick. The average composition for all samples was checked using a Rigaku X-ray fluorescence spectrometer. The resultant composition of the IPCM was found to be Ge 23 at.%, Sb 21 at.% and Te 56 at.%.

A Pulstec 100 dynamic disc unit was used to assess the ability to fully erase (corresponding to a 20 dB drop in the erasability) RESET bits of length 500 nm as a function of disc linear velocity. The discs were initialised with a continuous wave, 650 nm laser whilst the disc was rotated with a constant linear velocity of 2 ms^{-1}. RESET marks were written at a rate of 6 MHz with a 50% duty cycle. The disc was rotated with a linear velocity of 6 ms^{-1} thus the resultant marks were 500 nm in length. As the disc velocity is increased, the bits are illuminated for shorter times leading to the eventual situation where the illumination time is shorter than the material RESET-SET transition time. Fig. S2 shows a plot of the ability to erase the RESET marks (Erasability) as a function of the DVD's linear velocity. For GST this occurred at approximately 7 ms^{-1}. By considering the 500 nm length of RESET material, the minimum SET time was found to be approximately 70 ns. In comparison it was possible to fully SET the IPCM's bits at a disc velocity of 16 ms^{-1} corresponding to a minimum REEST-SET transition time of 30 ns. The IPCM showed a slightly lower erasability modulation in comparison to the GST film due to the inclusion of the Sb_2Te_3 nucleation layer. These results are consistent with those displayed in Fig. 1 that show the IPCM can be SET in approximately half of the time required by GST. Again, the IPCM shows a more abrupt response to the applied laser energy, suggesting a more coherent switching process.

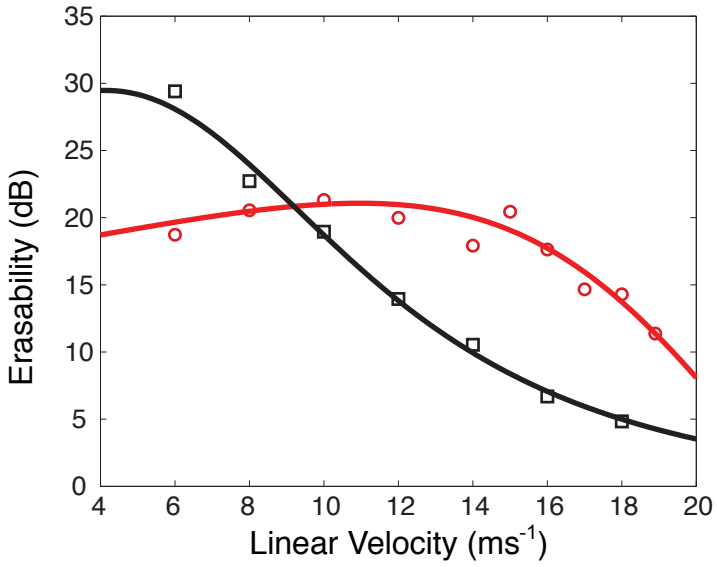

FIG. S2: DVD media speed comparison. Erasability of 500 nm long RESET marks as a function of disc linear velocity for GST (black) and $(GeTe)_2/(Sb_2Te_3)$ IPCM (red) films.

PCRAM Device Analysis

The device testing protocol consisted of applying SET and RESET pulses with the voltages given in Table S1. The SET pulse durations was 50 ns for the IPCM based devices and 100 ns for devices employing a GST material. Both devices were RESET with a 50 ns pulse. The resistance value was probed by applying a fixed voltage pulse of 500 ns duration and measuring the I-R data set. This measurement was repeated with a Log_{10} sampling of SET-RESET cycles. The $(GeTe)_2/(Sb_2Te_3)_2$ and $(GeTe)_4/(Sb_2Te_3)_2$ IPCM structures could endure more than 10^9 and 10^7 cycles respectively. This is a substantial improvement over the 1 - 2 $\times$ 10^6 cycle limit of the GST material. This enhanced cycle-ability is explained by a RESET operation that doesn't require the IPCM structure to melt. This is apparent from the TEM images of a cell cycled 1000 times and terminated in the RESET state, see Fig. 3(a). The TEM images and associated diffraction patterns show that the layered structure can withstand cycling. The lack of an amorphous dome in Fig 3(a) indicates that the material undergoes a solid-solid transition without melt-quenching. The selective area diffraction (SAD) patterns which were taken from different points within a PCRAM prove that the whole IPCM structure remains ordered. Fig. 3(b) shows the crystalline structure oriented at an angle with respect to Fig. 3(c-e). This problem tends to occur for thicker IPCM films (especially when the TiN heating electrode protrudes from the SiO2 layer). The SAD peaks collected from an area covering the majority of the IPCM (Fig. 3(f)) were compared with diffraction peaks calculated for a model of the $(GeTe)_2(Sb_2Te_3)_4$ IPCM structure that was relaxed by density

functional theory. The IPCM was assumed to go through the non-melting structural transition shown Fig. S1(c) with the Ge atoms tetrahedrally coordinated at the interface of the Sb_2Te_3 and GeTe layers. The measured separation of diffraction planes (Fig. 3(f)) were in good agreement (Fig. 3(g)) with values obtained from analysing the diffraction pattern of the relaxed $(GeTe)_2(Sb_2Te_3)_4$ IPCM model, shown in Fig.3(h). This model, therefore, gives plausible insight into the non-melting switching mechanism. For the DFT calculation, the atomic positions of 24 atoms in a IPCM $(GeTe)_2(Sb_2Te_3)_4$ supercell were optimised with respect to energy using the local density approximation and the plane wave DFT code CASTEP[8]. Norm-conserving pseudopotentials containing the 4p and 4s states of Ge and the 5s and 5p states of Sb and Te were used with a 230 eV energy cutoff.

Energy dispersive X-Ray fluorescence spectroscopy was used to analyse the composition of the $(GeTe)_4/(Sb_2Te_3)_2$ IPCM within a device. The device was cycled and terminated in the reset state before the point of typical failure. The composition of the device was measured directly above the heating electrode, in the centre of the cell and directly below the top electrode. Table S2 shows a comparison between the measured composition and the calculated average composition of the structure.

Table 1: Comparison between GST deposited from a composite target and the engineered IPCM

	$Ge_2Sb_2Te_5$ Composite	$GeTe/Sb_2Te_3$ iPCM
Device SET Voltage	3.0 V	1.5 V
Device RESET Voltage	6.0 V	3.5 V
Device SET Current (at 10^6 cycles)	0.30 mA	0.15 mA
Device RESET Current (at 10^6 cycles)	1.25 mA	0.73 mA
Cycle Lifetime	1 - 2 $\times 10^6$	> 2 $\times 10^7$
Device RESET Energy	375 pJ	255 pJ
Device SET Energy	90 pJ	11 pJ
Static Tester Recrystallisation Energy	950 pJ	380 pJ
Static Tester Crystallisation Time	> 80 ns	> 25 ns
DVD Tester Crystallisation Time	> 70 ns	> 30 ns
Perpendicular Thermal Conductivity	0.21 $Wm^{-1}K^{-1}$	0.33 $Wm^{-1}K^{-1}$

Table 2: Composition of the $(GeTe)_2(Sb_2Te_3)_4$ IPCM measured at thee points within a PCRAM device after cycling.

	Ge at. %	Sb at. %	Te at. %
Top	9	34	57
Middle	8	35	57
Bottom	7	34	60
Desired Composition	8.3	33.4	58.3

Thermoreflectivity Measurement

A pico-second resolution thermoreflectivity technique [9–12] was used to measure the thermal conductivity of the GST and IPCM films in their RESET states. The 30 nm thick phase change materials were sandwiched between 100 nm Mo layers atop of 1 mm thick fused silica substrates. A 500 ps, 30 mW, 1064 nm pump laser was incident on the sample's front surface whilst a 782 nm, 500 ps and 0.2 mW probe laser was incident on the sample's back surface. Calibrated reflectivity-temperature data were used to measure the temperature rise of the Mo layer. Fig. S3 shows the increase in temperature at the back surface of IPCM (red curve) and GST (black curve) samples. The rate of temperature increase with respect to time is clearly greater for the IPCM sample indicating that the IPCM has a higher thermal conductivity than GST.

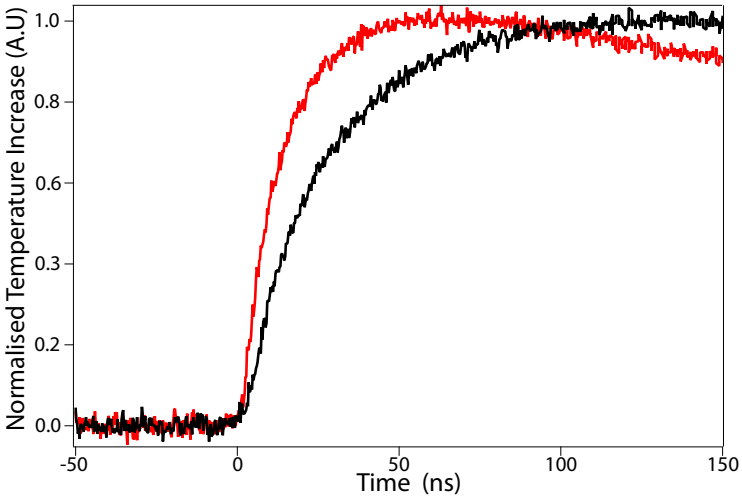

FIG. S3: Comparison of thermal conductivities. Normalised temperature increase at the back surface of GST (black) and IPCM (red) samples in their RESET state due to laser heating the film's front surface. The thermal conductivities were calculated to be 0.33 $Wm^{-1}K^{-1}$ for the IPCM and 0.21 $Wm^{-1}K^{-1}$ for the composite film.

[1] Chattopadhyay, T., Boucherle, J., and Von Schnering, H. Neutron diffraction study on the structural phase transition in GeTe. *J. Phys. C* **20**, 1431–1440 (1987).

[2] Sakai, N., Kajiwara, T., Takemura, K., Minomura, S., and Fujii, Y. Pressure-induced phase transition in Sb_2Te_3. *Solid State Commun.*. **40**(12), 1045–1047 (1981).

[3] Kifune, K., Kubota, Y., Matsunaga, T., and Yamada, N. Extremely long period-stacking structure in the Sb-Te binary system. *Acta Cryst. B* **61**, 492–497 (2005).

[4] Braun, W., Shayduk, R., Flissikowski, T., Ramsteiner, M., Grahn, H. T., Riechert, H., Fons, P., and Kolobov, A. Epitaxy of Ge-Sb-Te phase-change memory alloys. *Appl. Phys. Lett.* **94**(4), 041902-1 – 041902-3 (2009).

[5] Simpson, R. E., Hewak, D. W., Fons, P., Tominaga, J., Guerin, S., and Hayden, B. E. Reduction in crystallization time of Sb:Te films through addition of Bi. *Appl. Phys. Lett.* **92**(14), 141921-1–141921-3 (2008).

[6] Burr, G. W., Breitwisch, M. J., Franceschini, M., Garetto, D., Gopalakrishnan, K., Jackson, B., Kurdi, B., Lam, C., Lastras, L. A., Padilla, A., Rajendran, B., Raoux, S., and Shenoy, R. S. Phase change memory technology. *J. Vac. Sci. Technol. B* **28**(2), 223–262 (2010).

[7] Málek, J. The applicability of Johnson-Mehl-Avrami model in the thermal analysis of the crystallization kinetics of glasses. *Thermochim. Acta.* **267**, 61–73 (1995).

[8] Clark, S., Segall, M., Pickard, C., Hasnip, P., Probert, M., Refson, K., and Payne, M. First principles methods using CASTEP. *Zeitschrift für Kristallographie* **220**, 567–570 (2005).

[9] Taketoshi, N., Baba, T., and Ono, A. Development of a thermal diffusivity measurement system for metal thin films using a picosecond thermoreflectance technique. *Meas. Sci. Technol.* **12**(12), 2064–2073 (2001).

[10] Baba, T. Analysis of one-dimensional heat diffusion after light pulse heating by the response function method. *Jpn. J. Appl. Phys.* **48**(5), 05FEB04-1–05EB04-9 (2009).

[11] Taketoshi, N., Baba, T., and Ono, A. Electrical delay technique in the picosecond thermoreflectance method for thermophysical property measurements of thin films. *Rev. Sci. Instrum.* **76**(9), 094903-1–094903-8 (2005).

[12] Taketoshi, N., Baba, T., Schaub, E., and Ono, A. Homodyne detection technique using spontaneously generated reference signal in picosecond thermoreflectance measurements. *Rev. Sci. Instrum.* **74**(12), 5226–5230 (2003).

[13] Huang, B. and Robertson, J. Bonding origin of optical contrast in phase-change memory materials. *Phys. Rev. B* **81**(2), 081204-1–081204-4 (2010).

[14] Akola, J., Jones, R. O., Kohara, S., Kimura, S., Kobayashi, K., Takata, M., Matsunaga, T., Kojima, R., and Yamada, N. Experimentally constrained density-functional calculations of the amorphous structure of the prototypical phase-change material $Ge_2Sb_2Te_5$. *Phys. Rev. B* **80**(2), 020201-1–020201-4 (2009).

[15] Shportko, K., Kremers, S., Woda, M., Lencer, D., Robertson, J., and Wuttig, M. Resonant bonding in crystalline phase-change materials. *Nature Mater.* **7**(7), 653–658 (2008).

[16] Kolobov, A., Fons, P., Frenkel, A., Ankudinov, A., Tominaga, J., and Uruga, T. Understanding the phase-change mechanism of rewritable optical media. *Nature Mater.* **3**(9), 703–708 (2004).

[17] Tominaga, J., Shima, T., Fons, P., Simpson, R., Kuwahara, M., and Kolobov, A. What is the origin of activation energy in phase-change films? *Jpn. J. Appl. Phys* **48**(3), 03A053-1–03A053-3 (2009).